Proc. Natl. Acad. Sci. USA
Vol. 94, pp. 13329–13334, November 1997
Physiology

Basolateral membrane targeting of a renal-epithelial inwardly rectifying potassium channel from the cortical collecting duct, CCD-IRK3, in MDCK cells

SOPHIE LE MAOUT*, MANUEL BREJON*, OLAV OLSEN†, JEAN MEROT*, AND PAUL A. WELLING†‡

*Department de Biologie Cellulaire et Moleculaire, Centre d'Etudes Saclay, France; and †Department of Physiology, University of Maryland, School of Medicine, Baltimore, MD

Communicated by Gerhard Giebisch, Yale University School of Medicine, New Haven, CT, September 11, 1997 (received for review March 10, 1997)

ABSTRACT **We recently cloned an inward-rectifying K channel (Kir) cDNA, CCD-IRK3 (mKir 2.3), from a cortical collecting duct (CCD) cell line. Although this recombinant channel shares many functional properties with the "small-conductance" basolateral membrane Kir channel in the CCD, its precise subcellular localization has been difficult to elucidate by conventional immunocytochemistry. To circumvent this problem, we studied the targeting of several different epitope-tagged CCD-IRK3 in a polarized renal epithelial cell line. Either the 11-amino acid span of the vesicular stomatitis virus (VSV) G glycoprotein (P5D4 epitope) or a 6-amino acid epitope of the bovine papilloma virus capsid protein (AU1) was genetically engineered on the extreme N terminus of CCD-IRK3. As determined by patch-clamp and two-microelectrode voltage-clamp analyses in *Xenopus* oocytes, neither tag affected channel function; no differences in cation selectivity, barium block, single channel conductance, or open probability could be distinguished between the wild-type and the tagged constructs. MDCK cells were transfected with tagged CCD-IRK3, and several stable clonal cell lines were generated by neomycin-resistance selection. Immunoprecipitation studies with anti-P5D4 or anti-AU1 antibodies readily detected the predicted-size 50-kDa protein in the transfected cells lines but not in wild-type or vector-only (PcB6) transfected MDCK cells. As visualized by indirect immunofluorescence and confocal microscopy, both the tagged CCD-IRK3 forms were exclusively detected on the basolateral membrane. To assure that the VSV G tag was not responsible for the targeting, the P5D4 epitope modified by a site-directed mutagenesis (Y2F) to remove a potential basolateral targeting signal contained in this tag. VSV(Y2F) was also detected exclusively on the basolateral membrane, confirming *bona fide* IRK3 basolateral expression. These observations, with our functional studies, suggest that CCD-IRK3 may encode the small-conductance CCD basolateral K channel.**

Vectorial transport of ions, solutes, and macromolecules across epithelial cells depends on the polarized expression of transport molecules on two distinct plasma membrane domains. Consider the secretion of potassium (K) by the renal cortical collecting duct (CCD) principal cell, a transport process that largely maintains K homeostasis. In these cells, the directed movement of K from the interstitium to the tubule lumen depends on the asymmetric distribution and operation of an active transport pump and several types of K channels (1). The Na/K-ATPase, specifically expressed on the basolateral membrane, actively transports K into the cell exclusively from the interstitium. Accumulated above electrochemical equilibrium, K then exits the principal cell through different types of K channels that are expressed on both apical and basolateral membranes (2–4). Because the electrochemical driving force for K exit at the apical membrane exceeds that of the basolateral membrane, K preferentially enters the tubule lumen, allowing net K secretion (5). The expression of functionally disparate K channels on the two different membrane domains increases the fidelity of the secretory process (6, 7). Apical membrane K channels, characterized by a near linear current–voltage relationship (weak inward rectifying properties), allow avid efflux into the tubule lumen and efficient K secretion (8, 9). In contrast, the major basolateral K channel exhibits inward rectification (10–12). Subsequently, the basolateral membrane K channels can maintain membrane potential and a favorable electrical driving force for apical K exit without significantly recycling K back to the interstitium. In these regards, the specific targeting and appropriate expression of functionally distinct K channels on the two discrete membrane domains plays an essential role in the K secretory process.

Recent insights from molecular cloning has begun to provide some clues to explain the basis for differential targeting, functional diversity, and disparate regulation of K channels in the collecting duct. As predicted from their similar voltage-independent behavior and inward-rectifying nature, the strongest molecular candidates for the apical and basolateral K channels in the CCD principal cell belong to an emerging K channel family called the inward rectifiers or Kir (13). First discovered by Ho and Hebert, functional observations strongly suggest that ROMK (Kir 1.1) encodes an important, perhaps not exclusive, functional unit of the apical K channel in the CCD (14). On the other hand, CCD-IRK3 (Kir 2.3), isolated by our group from CCD cells, exhibit many of the functional properties of the basolateral K channel (15). Despite these breakthroughs, the lack of isoform-specific immunogenic structure in these CCD Kir channels has made their precise subcellular distribution difficult to elucidate by conventional immunocytochemistry with "isoform-specific" antibodies.

In the present study, an epitope-tag approach was employed to study membrane-targeting and polarized expression of CCD-IRK3 in an epithelial cell line, MDCK. In these cells, CCD-IRK3 is specially targeted to and expressed on the basolateral membrane. The observation provides further evidence for the role of CCD-IRK3 in the CCD principal cell and K homeostasis.

EXPERIMENTAL PROCEDURES

Construction of Epitope-Tagged IRK3 Channels. Three different tagged CCD-IRK3 channels were constructed by

The publication costs of this article were defrayed in part by page charge payment. This article must therefore be hereby marked "*advertisement*" in accordance with 18 U.S.C. §1734 solely to indicate this fact.

Abbreviations: CCD, cortical collecting duct; VSV, vesicular stomatitis virus; endo H, endoglycosidase H; PNGase, *N*-glycosidase F.

‡To whom reprint requests should be addressed at: Department of Physiology, University of Maryland, School of Medicine, 655 West Baltimore Street, Baltimore, MD 21201. e-mail: pwelling@umabnet.ab.umd.edu.

introducing three distinct epitopes onto the extreme N terminus of the CCD-IRK3 coding region. Each was engineered, with PCR *in vitro* mutagenesis, by inserting the nucleotide sequences encoding each epitope immediately after the initiation codon of CCD-IRK3. The epitope nucleotide sequences encode (*i*) the 11-amino acids of the vesicular stomatitis virus (VSV) G protein (YTDIEMNRLGK), (*ii*) a modified VSV G protein (*F*TDIEMNRLGK) epitope in which a potential basolateral sorting signal was disrupted by replacing the tyrosine with a phenylalanine (italic type) (16–18), or (*iii*) the 6-amino acid sequence encoding the AU1 epitope of the bovine papilloma virus capsid protein (DTYRYI). Both VSV G protein sequences are recognized by the P5D4 monoclonal antibody (Sigma) (16). The capsid protein epitope is detected by the AU1 monoclonal antibody (Babco, Richmond, CA) (19). Each of the epitope-tagged CCD-IRK3 cDNAs were sequenced with chain-terminating inhibitors (20) and Sequenase to verify proper construction. ORFs were subsequently subcloned into the expression vector Pcb6 containing the G418-resistance gene (17) for generation of the epitope-tagged CCD-IRK3/MDCK cell lines. For functional expression studies in *Xenopus* oocytes, the CCD-IRK3 constructs were subcloned between 5′ and 3′ untranslated regions of *Xenopus* β-globin in a modified SP64T plasmid (21), as we have done for the wild-type channel (15).

Transfection and Stable CCD-IRK3/MDCK Cell Line Generation. MDCK cells were plated at a density of 2×10^5 cells per 35-mm plastic dish and grown in DMEM supplemented with 10% fetal bovine serum at 5% CO_2 and 37°C. Epitope-tagged CCD-IRK3.Pcb6 recombinant plasmids were purified by CsCl gradient centrifugation. One day after seeding, the MDCK cells were transfected with 5 μg of tagged CCD-IRK3.Pcb6 recombinant plasmid by using Lipofectamine (BRL) according to the manufacture's specifications. The cells were trypsinized, diluted in DMEM (25:1), and seeded onto 100-mm Petri dishes 48 h after transfection. Stable transfected clones were isolated in a selection medium containing G418 (BRL; 500 μg/ml). Control cell clones were obtained by the same transfection protocol using the Pcb6 plasmid alone. Prior to all the experiments described in this study, the cells were treated overnight with 10 mM sodium butyrate to increase channel expression (22).

Metabolic Labeling, Immune Purification, and Immunoblot Analysis. For immunoprecipitation experiments, confluent MDCK cells, grown on permeable supports, were washed once with and then incubated at 37°C for 0.5 h in cysteine- and methionine-free DMEM (GIBCO/BRL). The cells were then incubated overnight at 37°C with 50 μCi/ml of [^{35}S]methionine and [^{35}S]cysteine (Express protein labeling mix, NEN; 1 Ci = 37 GBq). After the pulse, the cells were rinsed twice in phosphate-buffered saline (PBS) at 4°C and disrupted in lysis buffer (150 mM NaCl/50 mM Tris/5 mM EDTA, pH 7.5), supplemented with 1% Triton X-100, 1 mM phenylmethylsulfonyl fluoride, and a protease inhibitor mixture [antipain (10 μg/ml)/leupeptin (10 μg/ml)/pepstatin (10 μg/ml)] (buffer A). Lysates were precleared by addition of a suspension of protein A insoluble slurry [100 μl, 50% (vol/vol), prewashed three times with the lysis buffer; Sigma] for 2 h at room temperature and centrifugated at 15,000 × *g* for 15 min. The supernatant was incubated overnight at 4°C with 100 μl of protein A-Sepharose and P5D4 (1:1,000 dilution) or AU1 (1:100 dilution) antibodies. The beads were then washed successively, once with buffer A, three times with lysis buffer supplemented with 0.5% Triton X-100 and 0.1% SDS, three times with NaCl 500 mM, and twice with 50 mM Tris (pH 8.0). The beads were boiled with Laemmli buffer, and the proteins were separated on 10% polyacrylamide gels that were processed for autoradiography and/or analyzed on a PhosphorImager (Molecular Dynamics). For glycosidase digestion, beads were incubated overnight at 37°C with 2.5 μl of *N*-glycosidase F (PNGase) F (0.5 unit) or with endoglycosidase H (endo H; 10^{-3} units) after pH adjustment to 5.5 with 1 M HCl.

Immunofluorescence Studies. Cells were grown on permeable supports until they formed a confluent monolayer. They were rinsed twice with PBS supplemented with 1 mM $CaCl_2$ and 1 mM $MgCl_2$ (PBSCM) and fixed with 3% paraformaldehyde for 30 min. Cultures were then washed three times with PBSCM and incubated 15 min in PBSCM containing 50 mM NH_4Cl. After washing, the cultures were permeabilized with 0.1% Triton X-100 in PBSCM for 30 min and then incubated 2 h with P5D4 (Sigma) (1:1,000 dilution) or AU1 (Babco) (1:100 dilution) antibodies in PBSCM supplemented with 1% BSA. After several washes, the cultures were incubated 30 min with rhodamine-conjugated goat anti-mouse IgG (1:200 dilution; Pierce) in the same buffer. Filters were washed with PBSCM, mounted in PBS/glycerol, and observed with a Leitz confocal microscope.

cRNA Synthesis. For *Xenopus* oocyte expression studies, complementary RNA was transcribed *in vitro* in the presence of capping analogue [G(5′)ppp(5′)G] from each of the CCD-IRK3.SP6 *Xba*I-linearized constructs (VSVG-, AU1-, and wt-CCD-IRK3) by using SP6 RNA polymerase (Ambion, Austin, TX; mMesSAGE mMACHINE). After DNase treatment, cRNA was purified by phenol/chloroform extraction and ammonium-acetate/ethanol precipitation. Yield and concentration were quantified spectrophotometrically.

Electrophysiological Studies. To compare the functional properties of the epitope-tagged CCD-IRK3 to those of the wild-type channel, voltage-clamp and patch-clamp experiments were performed on *Xenopus* oocytes injected with channel cRNA. Standard protocols were followed for the isolation, care, and injection of *Xenopus laevis* oocytes as described (15). Whole cell oocyte currents were monitored by using a two-microelectrode voltage clamp equipped with a bath-clamp circuit (OC-725B, Warner, New Haven, CT) as described in detail (15). For these studies, oocytes were placed in a small Lucite chamber and continually superfused with a Ca- and Na-free buffer (85 mM *N*-methyl-D-glutamine/5 mM KCl/1 mM $MgCl_2$/5 mM Hepes, pH 7.4) at room temperature (21–25°C). For some experiments, K was replaced equal molar Na, keeping the monovalent cation concentration at 90 mM. Voltage-sensing and current-injecting electrodes had resistances of 0.5–1.5 MΩ when back filled with 3 M KCl. Stimulation and data acquisition were performed with a Macintosh Centris 650 computer using an Instrutech ITC16 A/D, D/A converter, and PULSE software.

For patch-clamp experiments in oocytes, the vitelline membrane was removed from oocytes after hyperosmotic shrinking as described by Methfessel *et al.* (23). Patch-clamp electrodes, pulled from glass capillary tubes (Corning no. 7052), had resistances of 0.5–10 MΩ when back filled with 140 mM KCl/1 mM $CaCl_2$/1 mM $MgCl_2$/10 mM Hepes, pH 7.4. Cell-attached recordings of single channels were made using an Axopatch 200A. Records were digitized using a VR-10B digital data recorder (Instrutech, Great Neck, NY) and were stored on a videotape. Single channel slope conductance was assessed by measuring single channel currents at holding potentials ranging from a membrane potential of −100 to 0 mV. Open probability was measured at a membrane potential of −80 mV.

Electrophysiological studies with MDCK cells were performed with cells grown on glass coverslips. The coverslips with adherent cells were transferred to a perfusion chamber mounted on an inverted microscope and perfused throughout the experiment with 140 mM KCl/1 mM $MgCl_2$/1 mM $CaCl_2$/5 mM glucose/10 mM Hepes, pH 7.4. Whole cell current recordings were performed by using pipettes (1–3 MΩ) filled with 140 mM KCl/1 mM $MgCl_2$/5 mM EGTA/10 mM Hepes, pH 7.2. In some studies, 120 mM external K^+ was replaced with Na (120 mM NaCl/20 mM KCl/1 mM $MgCl_2$/1

mM $CaCl_2$/5 mM glucose/10 mM Hepes, pH 7.4). Stimulation, data acquisition, and data analysis were performed by using PCLAMP6 software. Leak and capacitive currents were subtracted on line using the P/8 procedure. Recorded currents were filtered at 1.5 kHz by using a low pass Bessel filter.

RESULTS

N-Terminal Epitope Linkage Does Not Alter CCD-IRK3 Function. Neither the AU1 nor the VSV-G epitope linked to the extreme N terminus appear to alter the functional properties of the CCD-IRK3 channel. As determined by two-microelectrode voltage clamp in *Xenopus* oocytes injected with CCD-IRK3 channel cRNA (Fig. 1), both epitope-tagged channels exhibit identical strong inward-rectifying properties and similar activation and inactivation kinetics as the wild-type CCD-IRK3 channel. Estimated by the shift in the reverse potential upon replacement of 5 mM K with equal molar Na, channel selectivity of K over Na was not altered by either epitope (Table 1). Likewise, each of the epitope-tagged channels and the wild-type channel exhibit identical sensitivity to barium block. Similar results were observed at the single channel level. As assessed by patch-clamp analysis, the single channel conductance and open probability were not altered by epitope tagging (Table 1). The lack of epitope-dependent functional effects offers compelling evidence that the tags do not alter channel structure, a prerequisite for the targeting studies.

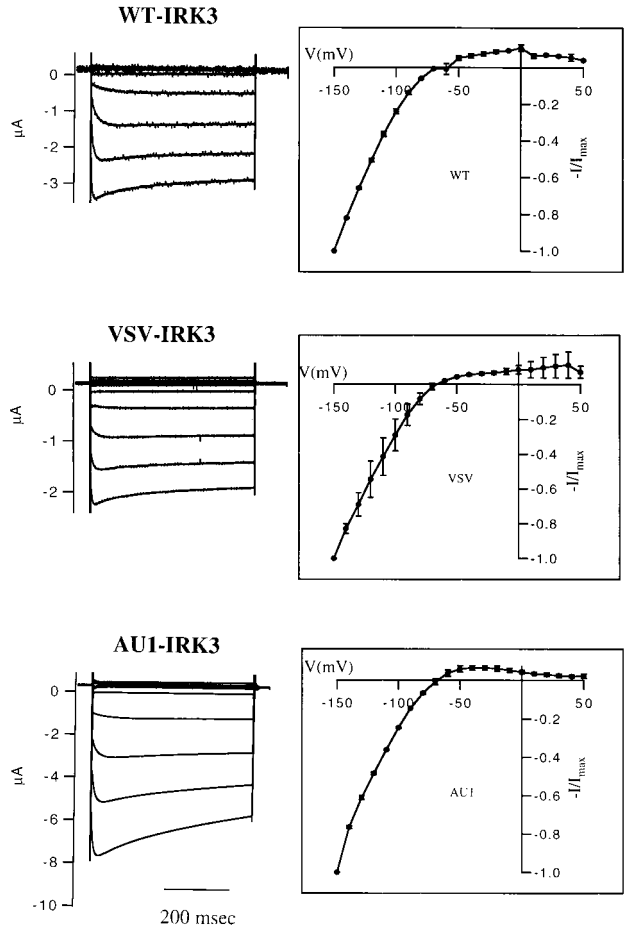

FIG. 1. N-terminal epitope tags do not alter the macroscopic properties of CCD-IRK3. Macroscopic K currents carried by the wild-type and VSV- and AU1-tagged channels in *Xenopus* oocytes are shown. Oocytes were held at O mV and pulsed in 10-mV increments from −150 to 50 mV. Families of current records from representative oocytes are shown on the left (current traces in 20-mV increments from −150 to 50 mV are shown). Current–voltage relationships for each of the channels are shown on the right.

Table 1. Epitope-tagged and wild-type channel selectivity

CCD-IRK3 type	γ, pS	P_o	P_K/P_{Na}	Barium block, % inhibition
Wild type	14 ± 2	0.81 ± 0.12	9.5 ± 6.0	86 ± 2
VSV tagged	14 ± 2	0.88 ± 0.23	12.1 ± 1.3	86 ± 1
AU1 tagged	11 ± 4	ND	9.4 ± 1.8	92 ± 3

γ, the single channel conductance was measured from the inward slope conductance in cell-attached patches (n = 3 of each). P_o, the open probability was near unity for the wild-type and VSV-tagged channels. Because the AU1-tagged channel appeared to exhibit similar high open probability kinetics, it was not quantified. The K-selectivity over Na P_K/P_{Na} was determined by the shift in the biionic reversal potential upon replacing 5 mM K with 5 mM Na in intact oocytes (n = 4 for each). Barium block was accessed by macroscopic analysis at −150 mV with 300 μM barium acetate in a 5 mM K bath. ND, not determined.

Functional Analysis of Epitope-Tagged CCD-IRK3 Channels in MDCK Cells. To determine whether the epitope-tagged channels are appropriately expressed in MDCK cells, the functional activity of each epitope-modified CCD-IRK3 channel was accessed in this polarized epithelial expression system using the whole-cell patch clamp technique. Fig. 2*A* illustrates a representative experiment for the VSV-Phe CCD-IRK3 channel. Analogous to CCD-IRK3 in *Xenopus* oocytes, transfected MDCK cells in symmetrical K (140 mM) exhibited strong inward rectifying properties. In contrast, no significant K currents were observed in mock-transfected cells. In the stable CCD-IRK3/MDCK cell lines, replacement of 120 mM extracellular K with Na (K + Na = 140 mM) shifted the reversal potential of the large inward rectifying currents by ≈50 mV, confirming high selectivity of K over Na ($P_K/P_{Na} \geq 10$). Likewise, the kinetics of activation and inactivation as well as the barium sensitivity of the tagged CCD-IRK3 channels were indistinguishable from the wild-type CCD-IRK3 channel in the oocyte expression system. In addition, the slow decrease in current amplitude during prolonged whole cell current recording and intracellular dialysis (data not shown) is reminiscent of channel rundown observed upon membrane patch excision in oocytes (15). Collectively, these observations, demonstrating that the three epitope-tagged CCD-IRK3 channels in MDCK cells and the wild-type channel in the oocyte expression system behave in an identical manner, support the notion that homomultimeric CCD-IRK3 channels are appro-

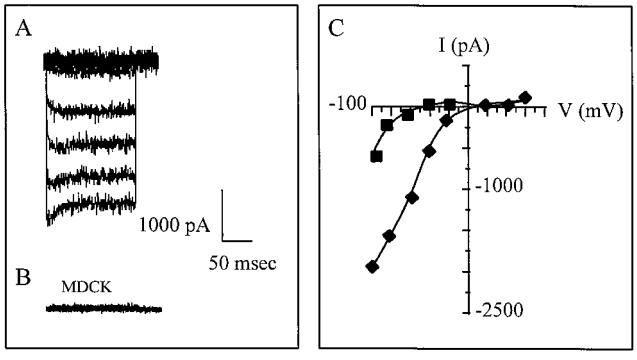

FIG. 2. Functional analysis of epitope-tagged IRK3 channels in MDCK cells. Typical whole cell currents recorded on VSV-IRK3-MDCK cells (*A*) and mock-transfected MDCK cells (*B*). The cells were bathed with high K^+ solution and voltage steps (200 msec) ranging from −100 to +80 mV were applied from a membrane holding potential of 0 mV. Similar whole cell currents were recorded on AU1- and VSV(Y2F)-IRK3-MDCK cells. (*C*) Current–voltage (I/V) plot of the whole cell currents recorded with high (140 mM) and low (20 mM) external K in VSV-IRK3-MDCK cells.

priately processed and delivered to the plasma membrane in MDCK cells.

Biochemical Analysis of CCD-IRK3 in MDCK Cells. To provide an independent test of appropriate CCD-IRK3 processing in MDCK cells, metabolic labeling and immunoprecipitation studies were performed. As shown in Fig. 3, both anti-AU1 and anti-VSV antibodies specifically recognize a protein with an apparent molecular weight of 57 kDa in epitope-tagged CCD-IRK3/MDCK cells but not in control cells. The size of the immunoprecipitated protein closely corresponds to the predicted molecular weight of the tagged CCD-IRK3 channel (50 kDa). As predicted from the lack of glycosylation consensus sites in the predicted ectodomain of CCD-IRK3, none of the immunoprecipited CCD-IRK3 polypeptides were sensitive to endo H or PNGase F digestion (Fig. 3). These studies demonstrate that the anti-epitope antibodies specifically recognize the CCD-IRK3 protein in MDCK cells. Furthermore, the CCD-IRK3 peptide immunoprecipitated by the anti-epitope antibodies appear to be fully maturated and appropriately processed.

Polarized Targeting of Tagged CCD-IRK3 Channel in MDCK Cells. After demonstrating that the epitopes do not alter the functional properties of the CCD-IRK3 channel and the anti-epitope antibodies specifically recognize the channel protein, the subcellular localization of CCD-IRK3 was determined in immunofluorescence experiments using laser scanning confocal microscopy. As illustrated on Fig. 4, VSV and AU1-tagged CCD-IRK3 channel proteins were exclusively localized on the basolateral membrane domain. To assure that the VSV G tag was not responsible for the targeting, the P5D4 epitope modified by a site-directed mutagenesis (Y2F) to remove a potential basolateral targeting signal contained in this tag. VSV (Y2F) was also detected exclusively on the basolateral membrane, making the distribution restricted to basolateral domain identical for each of the epitope-tagged channels and confirming *bona fide* CCD-IRK3 basolateral expression. No staining was observed in mock-transfected cells.

DISCUSSION

Renal K secretion and K homeostasis depend on the polarized expression of functionally distinct Kir channels on two separate plasma membrane domains of the CCD principal cell (1, 6). Although the identification of candidate K channel genes has begun to provide some clues to explain the basis for functional diversity and differential targeting of the channels involved in extracellular K balance (14, 15, 24), the precise subcellular location of these channels has remained unknown. Efforts to study of their distribution with conventional immunocytochemical approaches have been hampered by the lack of isoform-specific immunogenic structure on the different CCD Kir channels to generate isoform-specific antibodies. To circumvent this problem in the present study, we employed an epitope-tag approach to follow the subcellular expression of the putative basolateral K channel CCD-IRK3 in MDCK cells, a polarized renal epithelial cell line.

As predicted by the functional similarities shared between CCD-IRK3 and the small-conductance Kir channel in the CCD principal cell (15), confocal microscopy analysis revealed that epitope-tagged CCD-IRK3 channels are expressed exclusively on the MDCK cell basolateral membrane. Identical basolateral membrane expression patterns were observed with the three different epitopes, making it improbable that the introduced tag sequences dictate the targeting or selective retention of the channel on the basolateral membrane. Certainly, the AU1 epitope, a 6-amino acid sequence of the bovine papillomia virus, contains no known sorting signal for polarized expression in epithelial cells (25). Perhaps more convincing, basolateral membrane expression of the P5D4 epitope-tagged CCD-IRK3 channel was maintained despite disruption of the basolateral membrane sorting signal sequence in the VSV G protein epitope (16, 17). Although we cannot exclude the remote possibility that the particular placement of these tags might alter or obsure endogenous sorting signals, our observations collectively suggest that basolateral membrane expression is determined by the native CCD-IRK3 channel itself, rather than as a consequence of the epitope.

Our electrophysiological and biochemical characterization of the tagged CCD-IRK3 channels provide support for this notion. As assessed in *Xenopus* oocytes, N-terminal epitope linkage had no effect on the functional properties of CCD-IRK3. Inward rectification, barium sensitivity, single channel conductance, and the kinetic properties of the three different epitope-tagged channels were identical to the wild-type CCD-IRK3. Likewise, the functional properties of each epitope-tagged channel in MDCK cells were indistinguishable from the wild-type channel expressed in *Xenopus* oocytes. The lack of

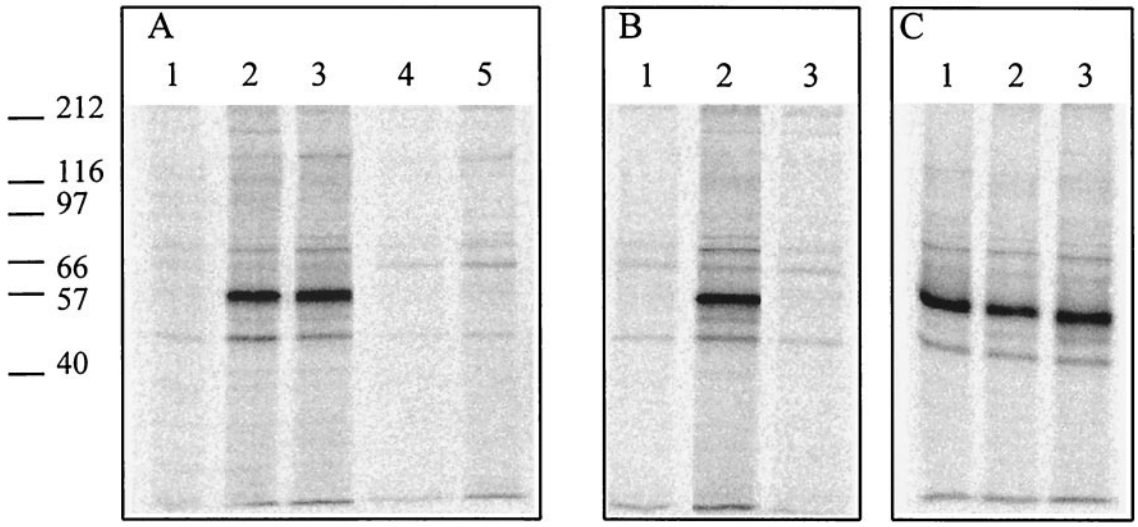

FIG. 3. Biochemical analysis of epitope-tagged IRK3 channels. Immunoprecipitation of radiolabeled tagged IRK3 channel proteins with P5D4 (*A*) and AU1 (*B*) antibodies. A specific 57-kDa band was immunoprecipitated in VSV, VSV(Y2F), and AU1-IRK3-MDCK cells (*A*, lanes 2 and 3, and *B*, lane 2, respectively) but not in the absence of P5D4 and AU1 antibodies (*A*, lanes 4 and 5, and *B*, lane 3, respectively) nor in MDCK cells (*A*, lane 1, and *B*, lane 1). (*C*) VSV-IRK3 protein (lane 1) was not sensitive to PNGaseF and endo H treatment (lanes 2 and 3, respectively). Numbers on the left indicate mobility of prestained molecular mass standards in kDa.

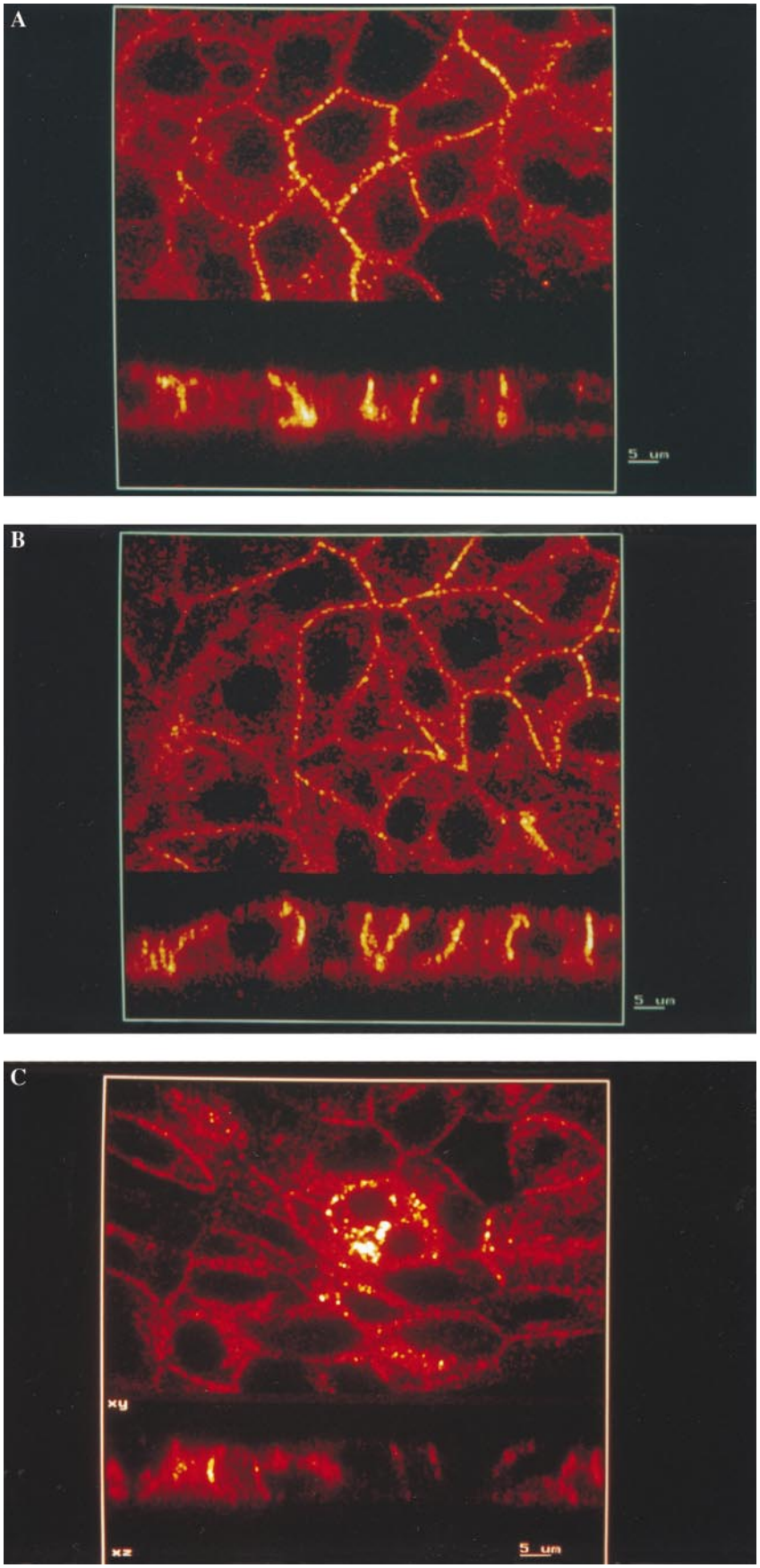

FIG. 4. Basolateral targeting of epitope-tagged IRK3 channels in MDCK cells. Immunolocalization of VSV, VSV(Y2F), and AU1-IRK3 channels in MDCK cells (*A–C*, respectively). The cells were grown to confluence on permeable supports and processed for immunofluorescence confocal microscopy. In each micrograph, *Upper* and *Lower* show horizontal and vertical sections through the cell layer, respectively. The yellow labeling of the basolateral cell membranes indicates specific targeting of the channel proteins to this membrane domain. (Bars = 5 μm.)

functional effect is consistent with the biochemical properties of the epitope-tagged channels. Metabolic labeling and immunoprecipitation studies revealed that the epitope-tagged channels are appropriately translated and expressed in MDCK cells. Indeed, each of the anti-epitope antibodies specifically immunoprecipitated a 57-kDa protein closely corresponding to the predicted molecular weight of the tagged CCD-IRK3 channels. Furthermore, because the only consensus sites for core glycosylation in the CCD-IRK3 protein reside in predicted endoplasmic domains, the resistance to glycopeptidase F and endo H treatment suggest the epitope-tagged channels are correctly folded in MDCK cells. Certainly, the requirement of Triton permeablization for CCD-IRK3 detection in immunofluorescence studies, predicted by the cytoplasmic orientation of N-terminal domain of CCD-IRK3, reinforce this contention. Collectively, these observations imply that the polarized basolateral membrane targeting of CCD-IRK3 in MDCK cells does not result from an epitope-induced change in channel structure. In this regard, it seems reasonable to assume that the wild-type CCD-IRK3 channel is normally targeted to and expressed on the basolateral membrane of MDCK cells. Because polarized sorting of some proteins may be dependent on the epithelial cell type (26), our results in the MDCK model obviously cannot be extrapolated to the native collecting duct with any certainty. Nevertheless, the close parallels in the functional properties of IRK3 and the native basolateral membrane K channel are consistent with basolateral membrane expression of IRK3 in the CCD.

Whether the restricted steady-state expression of CCD-IRK3 reflects the sorting and specific targeting of the channel from the level of the trans-Golgi network or random delivery to both membranes and selective retention in the basolateral membrane remains unknown. Unfortunately, the lack of primary amines in the predicted cytoplasmic domain of CCD-IRK3 precluded an answer to this question by biotinylation targeting studies. In any regard, both models predict that the signal for basolateral sorting is embedded within the structure of CCD-IRK3. Alternatively, CCD-IRK3 may assemble with undefined basolateral membrane targeting protein(s). We favor the former hypothesis for several major reasons. (*i*) Recent observations from our laboratory (22) and others (27) indicate that basolateral targeting of voltage-dependent K channels is determined by specific sorting signals located within the cytoplasmic C terminus of Kv-type channels. (*ii*) Observations from patch-clamp experiments in this study and Northern blot analysis (15), indicating that endogenous Kir channel expression is negligible in MCDK cells, make heteromultimeric assembly of CCD-IRK3 subunits with other Kir channels unlikely. Finally, although basolateral sorting signals are diverse and not well defined, CCD-IRK3 contains a motif at the extreme C terminus, characterized by a tyrosine and a downstream cluster acidic residues, that is similar to a basolateral targeting signal in the low density lipoprotein receptor (28, 29). Although intriguing, further study is obviously necessary before the domain in the CCD-IRK3 channel is deemed responsible for basolateral membrane sorting.

In conclusion, the major observation that CCD-IRK3 is exclusively expressed on the basolateral membrane of MDCK cells offers supportive evidence that CCD-IRK3 may encode the small-conductance basolateral-membrane K conductance in CCD principal cells. The development of this model system opens avenues to elucidate the molecular mechanisms involved in polarized targeting of Kir channels in renal epithelia, work that is certain to help resolve the molecular basis for K homeostasis.

We are grateful to Luc Morat (Centre à l'Energie Atomique) for technical assistance, to Raymond Hellio for expert help and advice with the confocal microscope, and to Dr. Evelyne Coudrier for helpful discussion. This project was funded in part with support from the University of Maryland School of Medicine and the National Institutes of Health (DK-48271).

1. Wright, F. S. & Giebisch, G. (1997) *The Kidney, Physiology and Pathophysiology*, eds. Seldin, D. W. & Giebisch, G. (Raven, New York), pp. 2249–2278.
2. Koeppen, B. M., Biagi, B. A. & Giebisch, G. H. (1983) *Am. J. Physiol.* **244,** F35–F47.
3. O'Neil, R. G. & Boulpaep, E. L. (1982) *Am. J. Physiol.* **243,** F81–F95.
4. O'Neil, R. G. & Sansom, S. C. (1984) *Am. J. Physiol.* **247,** F14–F24.
5. Sansom, S. C. & O'Neil, R. G. (1985) *Am. J. Physiol.* **248,** F858–F868.
6. Wang, W., Sackin, H. & Giebisch, G. (1992) *Annu. Rev. Physiol.* **54,** 81–96.
7. Hirsch, J. & Schlatter, E. (1995) *Kidney Int.* **48,** 1036–1046.
8. Frindt, G. & Palmer, L. G. (1989) *Am. J. Physiol.* **256,** F143–F151.
9. Wang, W., Schwab, A. & Giebisch, G. (1990) *Am. J. Physiol.* **259,** F494–F502.
10. Wang, W. H., McNicholas, C. M., Segal, A. S. & Giebisch, G. (1994) *Am. J. Physiol.* **266,** F813–F822.
11. Schlatter, E., Lohrmann, E. & Greger, R. (1992) *Pflugers Arch.* **420,** 39–45.
12. Lu, M. & Wang, W. H. (1996) *Am. J. Physiol.* **270,** C1336–C1342.
13. Doupnik, C. A., Davidson, N. & Lester, H. A. (1995) *Curr. Opin. Neurobiol.* **5,** 268–277.
14. Ho, K., Nichols, C. G., Lederer, W. J., Lytton, J., Vassilev, P. M., Kanazirska, M. V. & Hebert, S. C. (1993) *Nature (London)* **362,** 31–38.
15. Welling, P. A. (1997) *Am. J. Physiol.*, in press.
16. Thomas, D. C., Brewer, C. B. & Roth, M. G. (1993) *J. Cell Biol.* **268,** 3313–3320.
17. Brewer, C. B. & Roth, M. G. (1991) *J. Cell Biol.* **114,** 413–421.
18. Thomas, D. C. & Roth, M. G. (1994) *J. Biol. Chem.* **269,** 15732–15739.
19. Lim, P. S., Jenson, A. B., Cowsert, L., Nakai, Y., Lim, L. Y., Jin, X. W. & Sundberg, J. P. (1990) *J. Infect. Dis.* **162,** 1263–1269.
20. Sanger, F., Nicklen, S. & Coulson, A. R. (1977) *Proc. Natl. Acad. Sci. USA* **74,** 5463–5467.
21. Krieg, P. A. & Melton, D. A. (1984) *Nucleic Acids Res.* **12,** 7057–7070.
22. Le Maout, S., Sewing, S., Coudrier, E., Elalouf, J., Pongs, O. & Merot, J. (1996) *Mol. Membr. Biol.* **1,** 143–147.
23. Methfessel, C., Witzemann, V., Takahashi, T., Mishina, M., Numa, S. & Sakmann, B. (1986) *Pflugers Arch.* **407,** 577–588.
24. Yao, X., Segal, A. S., Welling, P., Zhang, X., McNicholas, C. M., Engel, D. & Desir, G. V. (1995) *Proc. Natl. Acad. Sci. USA* **92,** 11711–11715.
25. Le Gall, A. H., Yeaman, C., Muesch, A. & Rodriguez-Boulan, E. (1995) *Semin. Nephrol.* **15**(4), 272–284.
26. Gu, H. H., Ahn, J., Caplan, M. J., Blakely, R. D., Levey, A. I. & Rudnick, G. (1996) *J. Biol. Chem.* **271,** 18100–18106.
27. Scannevin, R. H., Murakoski, H., Rodhes, K. J. & Trimmer, J. S. (1996) *J. Cell Biol.* **135,** 1619–1632.
28. Hunziker, W., Harter, K., Matter, K. & Mellman, I. (1991) *Cell* **66,** 907–920.
29. Matter, K., Hunziker, W. & Mellman, I. (1992) *Cell* **71,** 741–753.